Science Advances
AAAS

advances.sciencemag.org/cgi/content/full/5/5/eaaw1874/DC1

Supplementary Materials for

Magnetizing topological surface states of Bi_2Se_3 with a CrI_3 monolayer

Yusheng Hou, Jeongwoo Kim, Ruqian Wu*

*Corresponding author. Email: wur@uci.edu

Published 31 May 2019, *Sci. Adv.* **5**, eaaw1874 (2019)
DOI: 10.1126/sciadv.aaw1874

This PDF file includes:

Part I. Main properties of the pristine and stretched monolayer CrI_3

We find that the small lattice stretch will not significantly affect all main properties of CrI_3 ML, including magnetic moments (M) of Cr^{3+} ions, band gap, magneto-crystalline anisotropy energy (MAE), and the nearest neighbor (J_1) and next nearest neighbor (J_2) Heisenberg exchange interactions (see table S1). Furthermore, as shown in the fig. S1, it also has almost no effect on the band structures of the monolayer CrI_3.

Table S1. Magnetic moment, bandgap, magnetocrystalline anisotropy energy, and Heisenberg exchange interactions J_1 and J_2.

a (Å)	M (μ_B/Cr)	Gap (eV)	MAE (meV/Cr)	J_1 (meV)	J_2 (meV)
7.04	3.0	1.03	0.488	-4.9576	-0.7848
7.22	3.0	1.08	0.544	-4.9816	-0.7415

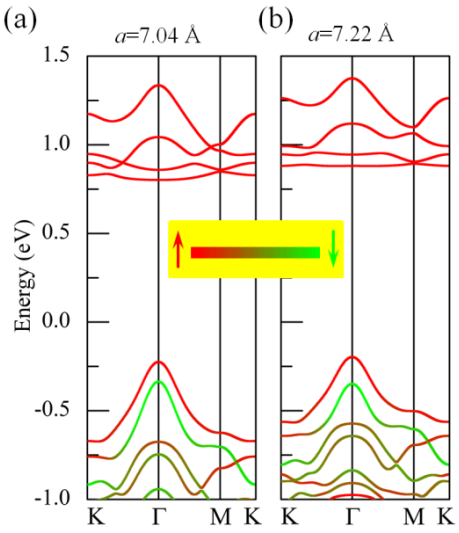

Fig. S1. DFT + SOC + *U*–calculated band structure of the CrI_3 ML with pristine and stretched lattice constants (a) a=7.04 Å (pristine) and (b) a=7.22 Å (stretched). The inset color bar shows the weight of spin-up (red) and spin-down (green) states.

Part II. Atomic alignment, binding energies and van der Waals gap of heterostructures $CrI_3/Bi_2Se_3/CrI_3$

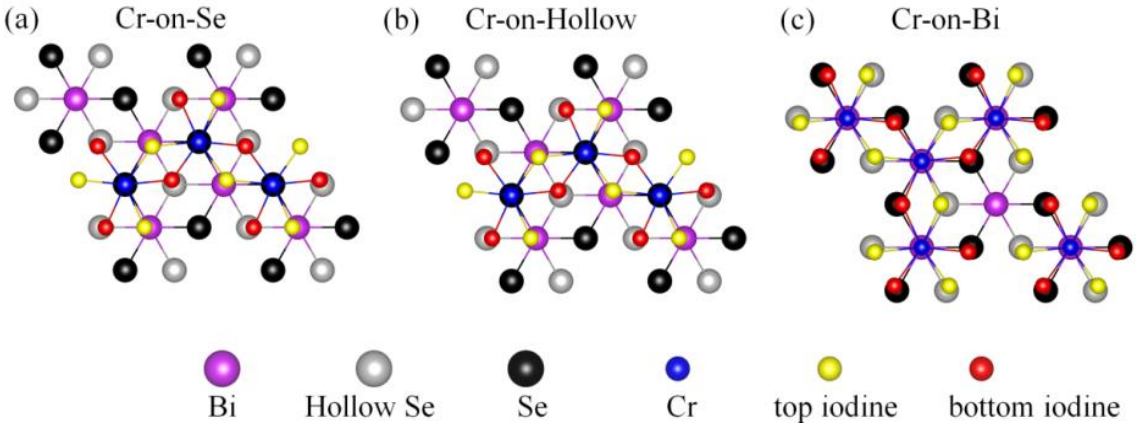

Fig. S2. Top views of the three highly symmetric alignments between CrI_3 and BS in $CrI_3/BS/CrI_3$ heterostructures. We denote the iodine layers of the monolayer (ML) CrI_3 closer to the topological insulator (TI) BS as the bottom iodine and its other iodine layers further away from TI BS as the top iodine. (**a**) The first alignment is Cr-on-Se, in which Cr atoms sit on the top of the Se atoms, the bottom iodine layers on the hollow and the top iodine layers on the top of Bi atoms. (**b**) The second alignment is Cr-on-Hollow, in which Cr atoms sit on the hollow formed by the Se atoms, the bottom iodine layers on the top of Bi atoms and the top iodine layers on the top of Se site. (**c**) The third alignment is Cr-on-Bi, in which Cr atoms sit on the top of the Bi atoms, the bottom iodine layers on top of Se atoms and the top iodine layer on the hollow.

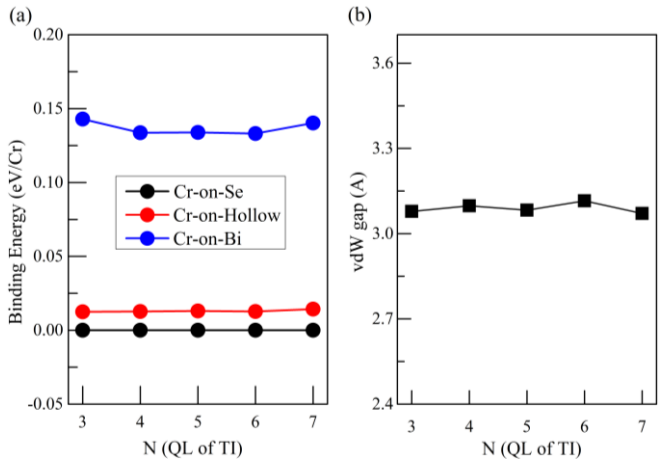

Fig. S3. Dependence of the binding energies and the vdW gaps CrI_3/BS/CrI_3 on the number (N) of QL of BS. (**a**) Dependence of the binding energies of the three highly symmetric alignments in heterostructures CrI_3/BS/CrI_3 on the quintuple layers (QLs) of BS. Binding energy is defined as $E_{binding} = E_{CrI_3/Bi_2Se_3/CrI_3} - E_{Bi_2Se_3} - E_{CrI_3}$ and we set the binding energy of the interface configuration Cr-on-Se as the reference. (**b**) Dependence of the van der Waals (vdW) gap of the most stable heterostructures CrI_3/BS/CrI_3 on the QLs of BS.

Part III. Topological properties of CrI_3/BS/CrI_3 with 4- and 5-QL BS studied by means of Wannier functions

From fig. S4 (a) and fig. S5 (a), we can see that the DFT calculated band structures of CrI_3/4QL-BS/CrI_3 and CrI_3/5QL-BS/CrI_3 are reproduced well. Especially, the four bands near the Fermi level around Γ point are reproduced exactly (see the insets in fig. S4 (a) and fig. S5 (a)). From fig. S4 (b), we can see there are non-negligible negative Berry curvatures around Γ point for CrI_3/4QL-BS/CrI_3. However, CrI_3/4QL-BS/CrI_3 only have huge positive Berry curvature appears (fig. S5 (b)). Here we calculate the Chern number C_N by integrating the Berry curvature in the first Brillion zone (FBZ). More explicitly

$$C_N = \frac{1}{2\pi}\frac{S_{FBZ}}{N}\sum_{i=1}^{N}\Omega_i \qquad (S1)$$

where S_{FBZ}, N and Ω are the area of FBZ, the number of sampled points in FBZ and Wannier functions calculated Berry curvature. Note that the points are even distributed in FBZ in Eq. (S1). If the points are not even distributed, their weight should be taken into account. For CrI_3/4QL-BS/CrI_3, 40000 points are even sampled in FBZ (fig. S4 (c)) and we get $C_N^{4QL} = 0$. For CrI_3/5QL-BS/CrI_3, its Berry curvature is extremely sharp around the Γ point. So 10000 points are sampled around the Γ point and 40000 points are sampled elsewhere (fig. S5 (c)), and we get $C_N^{5QL} = 1$

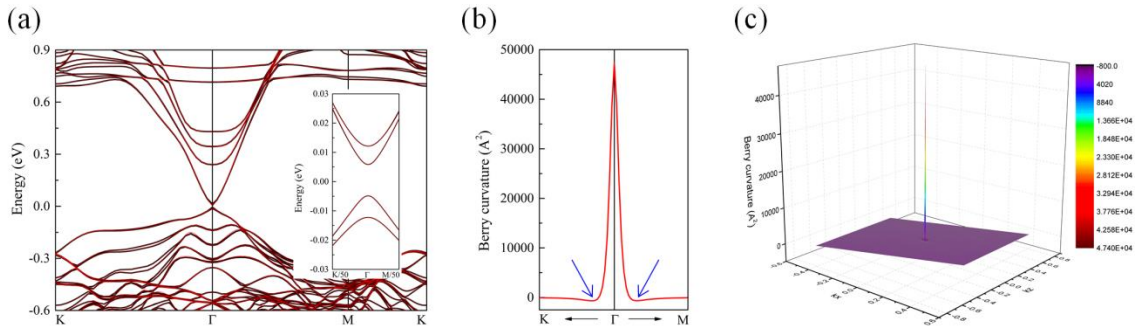

Fig. S4. Topological properties of CrI_3/4QL-BS/CrI_3. (a) DFT calculated (black lines) and Wannier functions reproduced (red lines) band structure. Inset shows the four bands near the Fermi level. (b) Wannier functions calculated Berry curvatures along the high-symmetric reciprocal paths. The non-negligible negative Berry curvatures are highlighted by the blue arrows. (d) Wannier functions calculated Berry curvatures in the first Brillouin zone.

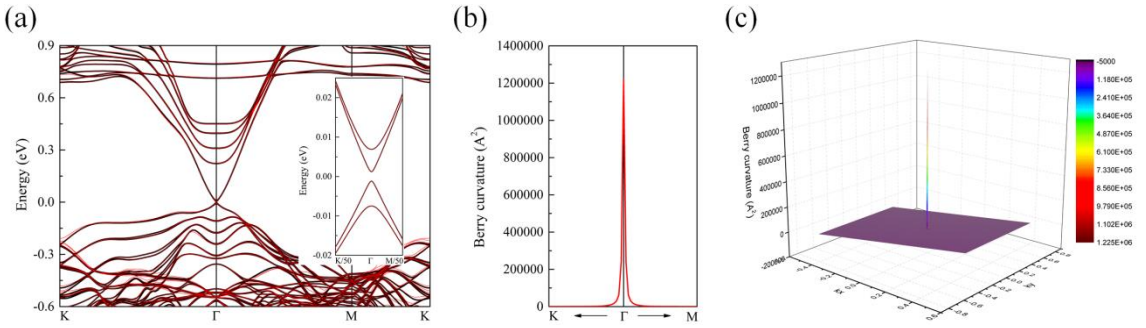

Fig. S5. Topological properties of CrI_3/5QL-BS/CrI_3. (a) DFT calculated (black lines) and Wannier functions reproduced (red lines) band structure. Inset shows the four bands near the Fermi level. (b) Wannier functions calculated Berry curvatures along the high-symmetric reciprocal paths. (d) Wannier functions calculated Berry curvatures in the first Brillouin zone.

Part IV. Fitted band structure of CrI_3/BS/CrI_3 heterostructures based on the effective four-band model

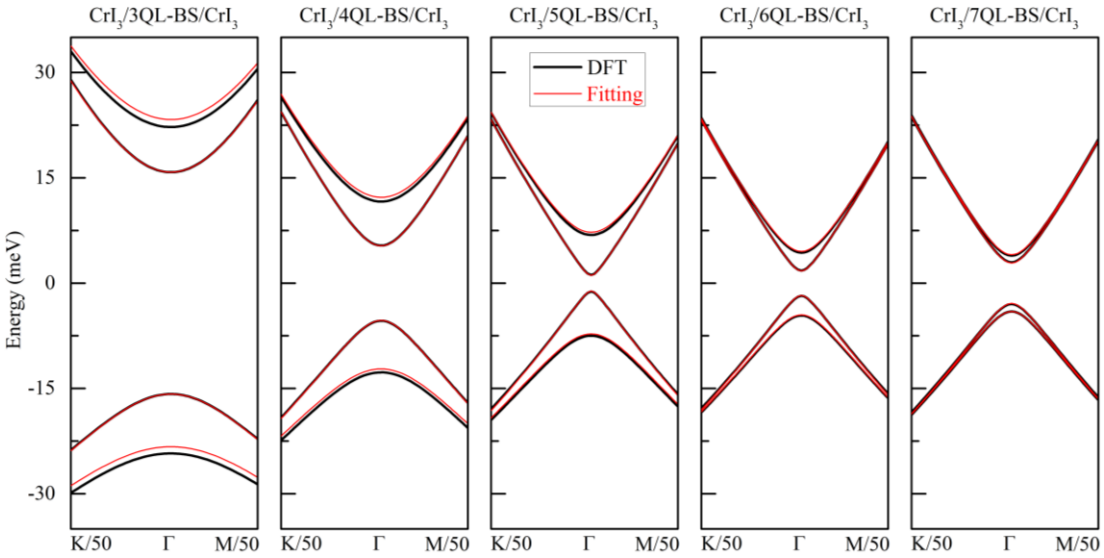

Fig. S6. DFT-calculated (black lines) and fitted band structures (red dashed lines) of CrI_3/BS/CrI_3 based on the effective four-band model (see Eq. 1 in the main text).

Table S2. Parameters of the effective four-band model (see Eq. 1 in the main text) are used to fit the DFT-calculated band of CrI_3/BS/CrI_3.

N (QL of BS)	vF (eV.Å)	M (eV)	B (eV.Å^2)	Δ (eV)	A (eV.Å^2)
3	1.841311	0.019554	2.995474	0.003745	18.304777
4	1.833892	0.008770	2.999848	0.003452	18.999006
5	1.781637	0.003069	2.999071	0.004173	18.995819
6	1.765403	0.001386	2.999949	0.003138	19.000093
7	1.800981	0.000591	2.999946	0.003466	19.000024

Part V. Band inversion analysis of the Hamiltonian Eq. (2) in the main text

Here we recall some important details of the Hamiltonian Eq. (2) in the main text. Within the new basis of the new basis of { $|+,\uparrow\rangle$, $|-,\downarrow\rangle$, $|+,\downarrow\rangle$ and $|-,\uparrow\rangle$ } with $|\pm,\uparrow\rangle=\left(|t,\uparrow\rangle\pm|b,\uparrow\rangle\right)/\sqrt{2}$ and $|\pm,\downarrow\rangle=\left(|t,\downarrow\rangle\pm|b,\downarrow\rangle\right)/\sqrt{2}$, the Hamiltonian Eq. (2) in the main text is

$$H\left(k_x,k_y\right)=A\left(k_x{}^2+k_y{}^2\right)+\begin{bmatrix} H_+\left(k_x,k_y\right) & 0 \\ 0 & H_-\left(k_x,k_y\right)\end{bmatrix}$$

In this equation, $H_\pm\left(k_x,k_y\right)=v_F k_y\sigma_x\mp v_F k_x\sigma_y+\left[\mathrm{M}\pm\Delta-B\left(k_x{}^2+k_y{}^2\right)\right]\sigma_z$ and $\sigma_{x,y,z}$ are Pauli matrices. Here, *t*, *b* denote the top and bottom surface states and $\uparrow$, $\downarrow$ represent the spin up and down states; v_F and $k_\pm=k_x\pm ik_y$ are the Fermi velocity and wave vectors, respectively; $M_k=\mathrm{M}-B\left(k_x{}^2+k_y{}^2\right)$ describes the coupling between the top and bottom TSSs and M is this coupling included gap; Δ is the exchange field from CrI_3. Note that $H_+\left(k_x,k_y\right)$ and $H_-\left(k_x,k_y\right)$ have opposite chirality. For $H_+\left(k_x,k_y\right)$, $\left(\mathrm{M}+\Delta\right)/B>0$ gives rise to band inversion; for $H_-\left(k_x,k_y\right)$, $\left(\mathrm{M}-\Delta\right)/B>0$ causes band inversion (5). Table 3 below lists the analysis of band inversions and Chern numbers C_N in $H_+\left(k_x,k_y\right)$ and $H_-\left(k_x,k_y\right)$ with respect to parameters Δ, M and *B*.

Table S3. Analysis of band inversions and the Chern number C_N with respect to parameters Δ, M and B.

		Δ	M	Band inverted in H_+	Band inverted in H_-	C_N of H_+	C_N of H_-	Total C_N
$B > 0$	$\Delta^2 > M^2$	> 0	> 0	Yes	No	1	0	1
		> 0	< 0	Yes	No	1	0	1
		< 0	> 0	No	Yes	0	-1	-1
		< 0	< 0	No	Yes	0	-1	-1
$B < 0$	$\Delta^2 > M^2$	> 0	> 0	No	Yes	0	1	1
		> 0	< 0	No	Yes	0	1	1
		< 0	> 0	Yes	No	-1	0	-1
		< 0	< 0	Yes	No	-1	0	-1

Part VI. The robustness of topological properties of CrI_3/BS/CrI_3 against U

Figure S7 shows the DFT calculated band structure and Berry curvature of CrI_3/BS-5QL/CrI_3 and CrI_3/BS-6QL/CrI_3 in the case of U=5 eV. We find that the gaps of CrI_3/BS-5QL/CrI_3 and CrI_3/BS-6QL/CrI_3 are 3.9 and 5.7 meV, respectively, which are comparable with the gaps of 2.3 and 3.6 meV in the case of U=3 eV. Such variances of the gaps may be due to the changed hybridizations between CrI_3 and BS which are affected by the choice of U. Therefore, the gaps of CrI_3/BS-5QL/CrI_3 and CrI_3/BS-6QL/CrI_3 are insensitive to the choice of U. Besides, by integrating the Berry curvature in the FBZ based on the Eq. (S1), we have that both Chern numbers of CrI_3/5QL-BS/CrI_3 and CrI_3/6QL-BS/CrI_3 are 1. This indicates that the change of U from 3 eV to 5 eV have no effect on the topological properties of CrI_3/BS/CrI_3. Taking these together, we conclude that the topological properties of CrI_3/BS/CrI_3 are very robust against the choices of U.

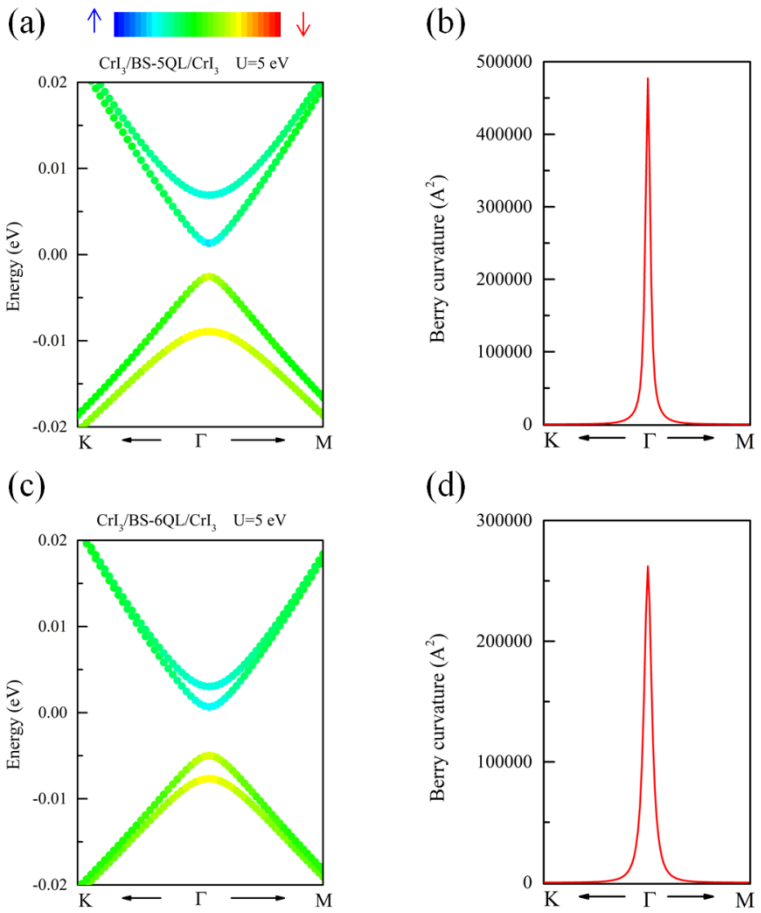

Fig. S7. Effect of *U* on the topological properties of CrI_3/BS/CrI_3. (a), (c) DFT calculated band and (d), (d) Berry curvature calculated by fitting the four-band model Eq. (1) in the main text for CrI_3/5QL-BS/CrI_3 and CrI_3/6QL-BS/CrI_3 when U=5 eV is used. The color bar in (a) indicates the spin projection weight in (a) and (b).